X-ray Scattering of Vinyl Polyolefin Liquids and Random Copolymers: Theory and Experiment

Huimin Li[†]

Department of Chemical Engineering, Colorado School of Mines, Golden, Colorado 80401

John G. Curro*

Department of Chemical & Nuclear Engineering, University of New Mexico, Albuquerque, New Mexico 87131

David T. Wu

Department of Chemistry & Department of Chemical Engineering, Colorado School of Mines, Golden, Colorado 80401

Anton Habenschuss

Chemical Sciences Division, Oak Ridge National Laboratory, Oak Ridge, Tennessee 37831

Received December 10, 2007; Revised Manuscript Received January 21, 2008

ABSTRACT: Polymer reference interaction site model (PRISM) calculations and wide-angle X-ray experiments were performed on vinyl polyolefin melts of polyethylene (PE), isotactic polypropylene (iPP), and poly(1-butene) (P1B). PRISM calculations were also carried out on poly(1-hexene) (P1H). For PE and iPP melts a single main peak in the scattering pattern was observed near wave vectors $k \sim 1$ Å^{-1}; for P1B and P1H we observed this main peak to split with the development of a prepeak that moves to lower wave vectors as the side chain size increased. By calculation of the various partial structure factors, we found that the prepeak formation is due to a combination of two effects: (1) an increase in the average distance between the chain backbones due to screening of the side chains and (2) increased intermolecular ordering of the pendant methyl groups as the side chains become longer. The scattering of random copolymers (PEP, PEB, PEH) of PE with iPP, P1B, and P1H, respectively, was also studied with PRISM theory as a function of composition. Development of a prepeak in the scattering from PEB and PEH was predicted to occur at copolymer compositions of less than 50% PE. No prepeak was predicted to occur at any composition in the PEP copolymer.

I. Introduction

With the discovery of new catalysts, the synthetic chemist now has unprecedented control over the macromolecular architecture of polyolefin polymers. This offers the possibility of optimizing polyolefin liquids, copolymers, and blends to have desired physical properties and processing characteristics. Recent studies have shown that the macromolecular architecture of polyolefins affects the molecular packing in the condensed state, which in turn controls many physical and thermodynamic properties. One important technique to characterize both the intermolecular and intramolecular packing of polymers is wide-angle X-ray scattering. In this paper we attempt to obtain a deeper understanding of the relationship between the X-ray scattering structure factor of polyolefins and their chain architecture.

Previous studies[1,2] of scattering from vinyl polymers showed systematic changes in the structural features of the main, wide-angle peak at wave vectors near $k \sim 1$ Å^{-1}. In polypropylene the main peak is broadened and shifted to lower wave vectors relative to polyethylene. Windle[3] observed that the single main peak seen in polyethylene actually splits into two peaks for polystyrene. The lower angle part of this split peak was referred to[3] as the *prepeak* by Windle. These structural features and trends were reproduced in the integral equation theory calculations of Curro[4] using the *polymer reference interaction site model* or PRISM theory on freely jointed, vinyl polymer chain melts. In this work we investigate the development of the prepeak in polyolefins by studying the scattering of vinyl polymers with successively larger pendant groups: polyethylene (PE), isotactic polypropylene (iPP), poly(1-butene) (P1B), and poly(1-hexene) (P1H). These polymers are shown schematically in Figure 1. We compare theoretical (PRISM) structure factors, using atomistically realistic models, with X-ray scattering experiments for PE, iPP, and P1B to explore the development of the prepeak. In addition, we also present PRISM theory calculations on P1H for the structure factor.

Polyolefin random copolymers are versatile materials that exhibit a wide range of physical properties as a function of copolymer composition. Random copolymers can also form

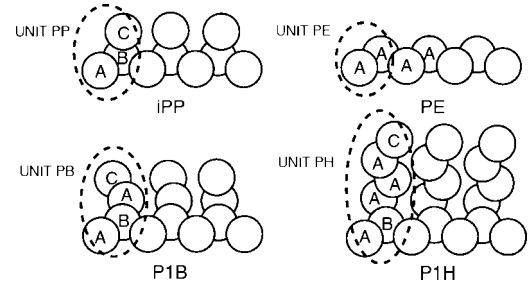

Figure 1. Schematic pictures of the polyolefin homopolymers studied in this investigation. A = CH_2, B = CH, and C = CH_3. The repeat units containing the united atom sites are indicated by the dashed curves.

* To whom correspondence should be addressed.
[†]Present address: Department of Chemistry, University of Tennessee, Knoxville, TN 37996.

10.1021/ma702748v CCC: $40.75
Published on Web 03/12/2008

Table 1. Experimental Polyolefin Samples

polymer	source	sample details
polyethylene[5,6] (PE)	Aldrich	$T = 423$ K, $M_w = 90$ kDa
isotactic polypropylene[1,2,10] (iPP)	Goodfellows Co.	$T = 453$ K, $M_v = 280$ kDa
isotactic poly(1-butene)[11] (P1B)	Scientific Polymer Products, Inc.	$T = 394$ K, $M_w = 21$ kDa

miscible blends with other polyolefin components.[5] For example, experiments[6,7] demonstrated that a miscibility window exists for iPP blended with random copolymers of PE and both P1B and P1H. PRISM calculations[8] by Li of the heats of mixing show miscibility windows in qualitative agreement with experiments for these systems. Thus, blend miscibility depends subtly on the chain architecture and packing of the random copolymer component. To develop an understanding of the relationship between chain structure and packing of random copolymers we also calculated the structure factor of the three random copolymers of PE with iPP, P1B, and P1H as a function of copolymer composition. Copolymers with both random and regularly spaced sequence distributions are examined.

We begin with brief descriptions of the experimental scattering measurements and the application of PRISM theory to polyolefin melts and copolymers. We then compare theory with experiments and speculate on the origin of the prepeak development in the pure component melts. We then show our theoretical predictions for changes in the structure factor for the three copolymers as the composition is varied between the pure components.

II. Experiment

A description of the samples of PE,[9,10] iPP,[1,2,11] and P1B[12] is given in Table 1. The X-ray intensities were measured from the free, horizontal sample surface on a Scintag PAD-X $\theta-\theta$ diffractometer using reflection geometry.[13] Mo Kα radiation ($\lambda = 0.7107$ Å, 50 kV, 40 mA) and a solid-state detector were used. Intensities were measured over a momentum transfer range of $0.3 < k < 16$ Å^{-1}, where $k = 4\pi\lambda^{-1}\sin\theta$, with 2θ the scattering angle.

As in earlier work.[1,9,10] the scattering data were corrected for polarization[14] and scattering volume dependent absorption.[15] The intensity curve was then corrected for monochromator discrimination,[16] incoherent scattering,[17] and multiple scattering.[18] The resulting corrected scattering intensity $I(k)$ is related to the partial structure factors $\hat{S}_{\alpha\gamma}(k)$ according to

$$I(k) = \sum_{\alpha\gamma=1}^{N_s} I_{\alpha\gamma}(k) = \sum_{\alpha\gamma=1}^{N_s} f_\alpha(k) f_\gamma(k) \hat{S}_{\alpha\gamma}(k)/\rho_\alpha \quad (1)$$

where N_s is the total number of sites within a repeat unit (see Figure 1) and $f_\alpha(k)$ is the coherent scattering factor[19] of a united atom site CH, CH_2, or CH_3. Our results were reported in terms of a modified structure function $H(k)$ obtained from $I(k)$ by subtracting the self-scattering $\hat{S}_s(k)$ from uncorrelated sites followed by normalizing to a repeat unit

$$H(k) = \frac{N_s(I(k) - \hat{S}_s(k))}{\left(\sum_{\alpha=1}^{N_s} f_\alpha(k)\right)^2} \quad (2)$$

where the self-scattering was obtained from

$$\hat{S}_s(k) = \sum_{\alpha=1}^{N_s} f_\alpha^2(k) \quad (3)$$

The X-ray scattering results of interest in the present investigation are displayed as the points in Figure 2 for PE, iPP, and P1B.

III. PRISM Theory

In this investigation we applied PRISM theory to compute the structure factors of the polyolefins displayed in Figure 1.

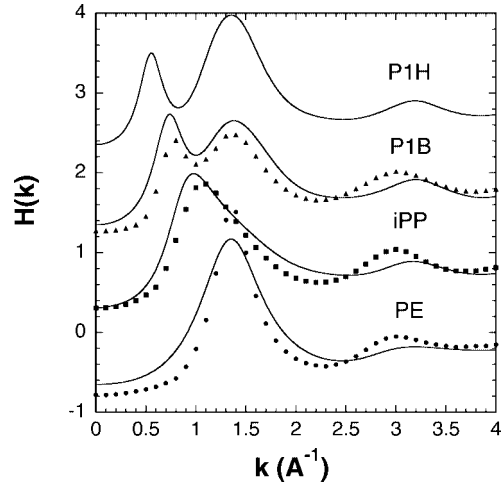

Figure 2. Structure function $H(k)$ (see eq 2) as a function of wave vector k measured and calculated for the various polyolefin melts indicated. The experimental X-ray scattering results are denoted by circles for PE, squares for iPP, and triangles for P1B. The theoretical results from PRISM theory are shown as solid curves. For clarity, the results for each polyolefin are displaced vertically by 1.0.

PRISM theory[20–22] is an extension to polymers of the RISM or *reference interaction site model* developed by Chandler and Andersen[23,24] for small molecule liquids. PRISM theory has been discussed in detail in earlier publications[25] and will only briefly be discussed here. Consider a polymer liquid consisting of $\tilde{\rho}$ chains per unit volume where each chain has N_α sites of type α and site density $\rho_\alpha = \tilde{\rho}N_\alpha$. The purpose of the theory is to self-consistently calculate both the intermolecular and intramolecular structure of the polymer liquid characterized by (1) the intermolecular pair correlation functions $g_{\alpha\gamma}(r)$ between pairs of sites of type α and γ on different polymer chains, and (2) the intramolecular distribution functions

$$\Omega_{\alpha\gamma}(r) = \tilde{\rho} \sum_{i\in\alpha,\, j\in\gamma} \omega_{ij}(r)$$

where $\omega_{ij}(r)$ is the normalized probability density between a pair of sites i and j along the same chain backbone. The theory makes use of the generalized Ornstein–Zernike equations[23,24] of Chandler and Andersen which can be compactly written in matrix notation in Fourier transform space

$$\hat{\mathbf{H}}(k) = \hat{\mathbf{\Omega}}(k) \cdot \hat{\mathbf{C}}(k) \cdot [\hat{\mathbf{\Omega}}(k) + \hat{\mathbf{H}}(k)] \quad (4)$$

where the carets denote Fourier transformation with wave vector k. In eq 4 $H_{\alpha\gamma}(r) = \rho_\alpha\rho_\gamma\,[g_{\alpha\gamma}(r) - 1]$ and $C_{\alpha\gamma}(r)$ are the direct correlation functions discussed below. The Fourier transform of $\Omega_{\alpha\gamma}(r)$ is identified with the single chain structure factors.

$$\hat{\Omega}_{\alpha\gamma}(k) = \tilde{\rho} \sum_{i\in\alpha, j\in\gamma}^{N} \left\langle \frac{\sin kr_{ij}}{kr_{ij}} \right\rangle \quad (5)$$

The summation in eq 5 is over intramolecular pairs of sites on a single chain. The Greek letters α or γ refer to the various site types CH, CH_2, and CH_3 making up the repeat units in the vinyl polyolefins depicted in Figure 1.

The generalized Ornstein–Zernike equation in eq 4 can be thought of as a definition for the intermolecular direct correlation functions $C_{\alpha\gamma}(r)$ in analogy with the theory of atomic liquids.[26] The application of PRISM theory to polymer liquids requires two approximations. The first is a closure relationship for the direct correlation functions. Since $C_{\alpha\gamma}(r)$ is a short-range function of r, we employ the well-known Percus–Yevick (PY) approximate closure from the theory of atomic liquids[25,26]

$$C_{\alpha\gamma}(r) \cong \{1 - \exp[\beta U_{\alpha\gamma}(r)]\} g_{\alpha\gamma}(r) \quad (6)$$

where $U_{\alpha\gamma}(r)$ is the nonbonded potential. Equation 6 can be used to eliminate the direct correlation function from eq 4, thus providing a relationship between the intermolecular packing $g_{\alpha\gamma}(r)$ and intramolecular structure $\Omega_{\alpha\gamma}(r)$ of the polymer liquid.

For a given intramolecular structure factor $\hat{\Omega}_{\alpha\gamma}(k)$, eqs 4 and 6 can be solved numerically for the intermolecular radial distribution functions. One could make use of Flory's ideality hypothesis[27] by approximating the single chain in a polymer melt as a chain without long-range excluded volume interactions. More exact calculations on flexible chains, however, require that the intramolecular structure be determined self-consistently with the intermolecular packing. This self-consistent computation proceeds by replacing the full many chain computation with a single chain Monte Carlo simulation in the potential energy field

$$U(\mathbf{R}) = U_E + W(\mathbf{R}) \quad (7)$$

where U_E represents the conventional bonded and nonbonded interactions that an isolated chain would experience. $W(\mathbf{R})$ is a medium-induced potential that mimics the effects of the other chains in the system. The essence of the Flory hypothesis[27] is that the repulsive excluded volume interactions and attractive medium induced potentials effectively cancel each other out in eq 7. In our second approximation in PRISM theory we take the medium-induced potential to be pairwise additive with the form[25,28,29]

$$\beta \hat{W}_{\alpha\gamma}(k) = -\sum_{i,j} \hat{C}_{\alpha i}(k)\, \hat{S}_{ij}(k)\, \hat{C}_{j\gamma}(k) \quad (8)$$

where the partial structure factors are defined as

$$\hat{S}_{\alpha\gamma}(k) = \hat{\Omega}_{\alpha\gamma}(k) + \hat{H}_{\alpha\gamma}(k) \quad (9)$$

The functional form of eq 8 can be motivated by viewing $\hat{W}_{\alpha\gamma}(k)$ as a potential of mean force (in Fourier transform space) arising from the HNC theory of atomic liquids.[25,26]

Equations 4−9 provide a set of relations that can be solved for both the intermolecular and intramolecular correlation functions for a particular choice of the site/site pair potentials. The calculation involves a single chain Monte Carlo simulation of $\hat{\Omega}_{\alpha\gamma}(k)$ required by eq 5. Since the medium induced potential depends on the intermolecular direct correlation functions and vice versa, it is necessary to solve the self-consistent problem iteratively. We use a Picard iteration procedure that has been described previously.[2] It is important to note that reweighting techniques can be employed so that the Monte Carlo simulation does not have to be repeated in each iteration.[2,30]

U_E in eq 7 contains both local bonding, bending and torsional potentials as well as longer range nonbonded potentials. In our application to polyolefins we used the Lennard-Jones potential between both intramolecular and intermolecular nonbonded sites.

$$U_{\alpha\gamma}(r) = 4\epsilon_{\alpha\gamma}\left[\left(\frac{\sigma_{\alpha\gamma}}{r}\right)^{12} - \left(\frac{\sigma_{\alpha\gamma}}{r}\right)^{6}\right] \quad (10)$$

For atomic liquids[26] and polymer melts[25] at liquidlike densities the liquid structure is primarily determined from the repulsive part of the potential. Consequently, we follow Weeks, Chandler, and Andersen[31] by dividing the total nonbonded potential into a repulsive part

$$U^{rep}_{\alpha\gamma}(r) = U_{\alpha\gamma}(r) + \epsilon_{\alpha\gamma}, \quad r \le r^*$$
$$U^{rep}_{\alpha\gamma}(r) = 0, \quad r \ge r^* \quad (11a)$$

and an attractive, or perturbative contribution

$$U^{att}_{\alpha\gamma}(r) = -\epsilon_{\alpha\gamma}, \quad r \le r^*$$
$$U^{att}_{\alpha\gamma}(r) = U_{\alpha\gamma}, \quad r \ge r^* \quad (11b)$$

where $-\epsilon_{\alpha\gamma} = U_{\alpha\gamma}(r^*)$ is the minimum value of the Lennard-Jones potential occurring at a separation $r = r^*$. Only the repulsive part (eq 11a) of the nonbonded potential was used in the self-consistent PRISM calculation since it has been found[25] to yield more accurate intermolecular pair correlation functions. In this investigation we employed the TraPPE united atom model of Martin and Siepmann.[32,33] Both the intramolecular (stretching, bending, and torsional) potentials and intermolecular Lennard-Jones parameters are displayed in Table 2 from this model.

Self-consistent solution of the PRISM theory as outlined above can be employed to determine the correlations in a liquid of any polymer that can be constructed from spherically symmetric sites. Of course, the number of independent $g_{\alpha\gamma}(r)$ and $\hat{\Omega}_{\alpha\gamma}(k)$ correlations needed to characterize the liquid increases, along with the computational time, with the number of sites N_s in the repeat unit according to $N_s(N_s + 1)/2$. The chain architecture enters the problem when a single chain Monte Carlo simulation is performed to compute $\hat{\Omega}_{\alpha\gamma}(k)$ as the average in eq 5. This single chain average was performed for the polyolefin repeat units shown in Figure 1. The total number of united atom sites (N_T) in the chain are specified in Table 4. In the case of the vinyl polymers iPP, P1B, and P1H the stereochemistry was constructed to be isotactic. All the calculations were performed at $T = 453$ K, above any of the experimental crystallization melting or glass transition temperatures. The densities used in the calculation[8] were within the experimental values at that temperature: PE,[34] iPP,[35] and P1H[36] had densities of 0.032 82 sites/Å^3 and P1B[35] had a density of 0.033 32 sites/Å^3. In our PRISM calculations on the copolymers of PE with iPP, P1B, and P1H, two sequence distributions were used in the Monte Carlo simulations: a randomly chosen distribution and a regular alternating distribution chosen to give a desired overall copolymer composition.

IV. Results and Discussion

A comparison of the PRISM calculations and wide-angle, X-ray scattering data is displayed in Figure 2 for the pure

Table 2. Potential Parameters for Polyolefins[32,33]

Lennard-Jones parameters	ϵ (kcal/mol)		σ (Å)	
CH	0.0198		4.68	
CH_2	0.0912		3.95	
CH_3	0.1944		3.73	
bond stretching $^1/_2 k_{bond}(l - l_0)^2$	l_0 (Å)		k_{bond} (kcal/(mol Å^2))	
CH_x−CH_y	1.54		900	
bending $^1/_2 k_{bend}(\theta - \theta_0)^2$	θ_0 (deg)		k_{bend} (kcal/(mol rad^2))	
CH_x−CH−CH_y	112		123.75	
CH_x−CH_2−CH_y	114		123.75	
torsion $\sum_{i=0}^{3} a_i \cos^i \varphi$	a_0 (kcal/mol)	a_1 (kcal/mol)	a_2 (kcal/mol)	a_3 (kcal/mol)
CH_x−CH−CH_2−CH_y	0.783	1.775	0.443	−3.500
CH_x−CH_2−CH_2−CH_y	2.007	4.012	0.271	−6.290
improper parameters $^1/_2 k_{impr}(\Psi - \Psi_0)^2$	Ψ_0 (deg)		k_{impr} (kcal/(mol rad^2))	
CH−CH_3, CH_2−CH_2	30.25		123.75	

Table 3. Copolymer Chains Used in the Present Calculations[a]

composition	PEP	PEB	PEH
$x = 0.25$	PP-3PE⋯	PB-3PE⋯	PH-3PE⋯
$x = 0.50$	PP-PE⋯	PB-PE⋯	PH-PE⋯
$x = 0.75$	3PP-PE⋯	3PB-PE⋯	3PH-PE⋯
		PEP	
$x = 0.25$	PP-PE-PP-6PE-PP-3PE-2PP-7PE-PP-3PE-PP-PE⋯		
$x = 0.50$	2PP-4PE-6PP-PE-PP-5PE-PP-PE-3PP-2PE⋯		
$x = 0.75$	4PP-2PE-5PP-PE-6PP-3PE-3PP⋯		
		PEB	
$x = 0.25$	3PE-PB-4PE-PB-3PE-PB-2PE-2PB-3PE⋯		
$x = 0.50$	PE-2PB-2PE-2PB-3PE-4PB-2PE⋯		
$x = 0.75$	2PB-PE-2PB-PE-3PB-2PE-5PB⋯		
		PEH	
$x = 0.25$	3PE-PH-4PE-PH-2PE-PH-PE-PH-2PE⋯		
$x = 0.50$	2PE-2PH-3PE-PH-PE-2PH-PE-2PH⋯		
$x = 0.75$	2PE-5PH-PE-4PH⋯		

[a] Regularly spaced sequences and parts of the randomly generated sequences are shown.

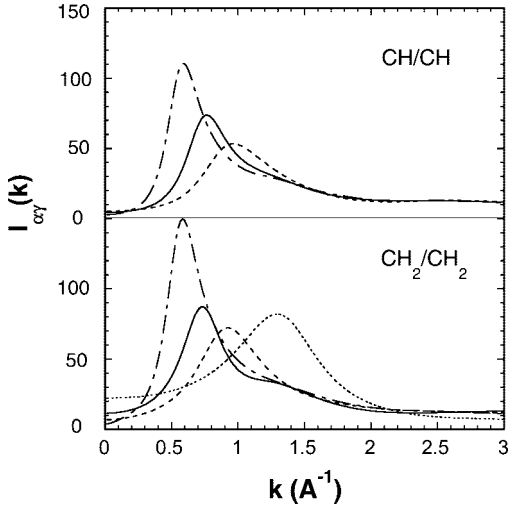

Figure 3. Partial contributions to the scattering intensity $I_{\alpha\gamma}(k)$ (see eq 12) from chain backbone sites calculated as a function of wave vector: PE (dotted curves), iPP (dashed curves), P1B (solid curves), and P1H (short/long dashed curves). Lower panel: α, $\gamma \Rightarrow CH_2$ sites; upper panel α, $\gamma \Rightarrow$ CH sites.

component melts of PE, iPP, and P1B. PRISM calculations for P1H are also shown although no X-ray scattering data were available. Good qualitative agreement between experiment and theory was observed. Clear trends were seen in both the scattering and theory in the low wave vector regime. In PE there is a main peak at $k \sim 1.4$ Å^{-1}. In iPP this main peak broadens and shifts to lower wave vectors ($k \sim 1.0$ Å^{-1}). As the pendant group increases in size in P1B, the main peak splits into two distinct peaks at $k \sim 0.75$ Å^{-1} and $k \sim 1.4$ Å^{-1}. This is similar to the peak splitting and prepeak observed[3] by Mitchell and Windle in polystyrene melts. Finally in P1H, where the pendant group is largest, the theory predicted that the prepeak shifted to a still lower wave vector $k \sim 0.55$ Å^{-1} while the other peak remained approximately in the same position at $k \sim 1.4$ Å^{-1}.

Let us now explore possible reasons for the peak splitting and emergence of a prepeak by looking at the partial contributions to the total scattering (eq 1)

$$I_{\alpha\gamma}(k) = f_\alpha(k)\, f_\gamma(k)\, \hat{S}_{\alpha\gamma}(k)/\rho_\alpha \qquad (12)$$

where $\hat{S}_{\alpha\gamma}(k)$ is the partial structure factor defined in eq 9. In Figure 3 we plotted the scattering contributions from pairs α and γ of sites CH and CH_2 along the main chains. It can be seen that these backbone contributions to the scattering mirror the prepeak behavior in Figure 2. The CH_2/CH_2 scattering peak moves to lower wave vectors (1.3, 0.93, 0.73, and 0.59 Å^{-1}) as

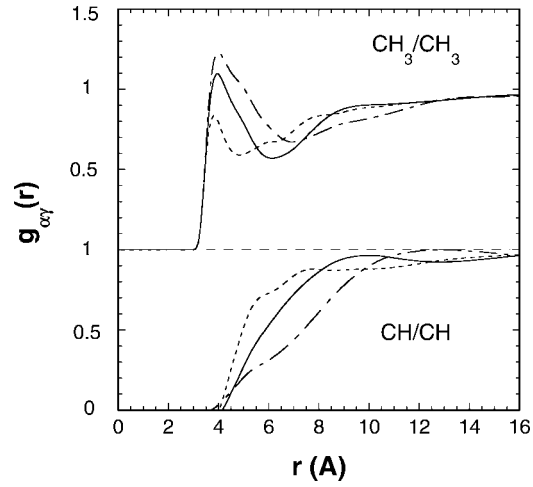

Figure 4. Intermolecular radial distribution function $g_{\alpha\gamma}(r)$ calculated for various vinyl polyolefin melts: dashed curves are for iPP, solid curves for P1B, and short/long dashed curves for P1H. Lower panel: α, $\gamma \Rightarrow$ CH sites; upper panel α, $\gamma \Rightarrow CH_3$ sites.

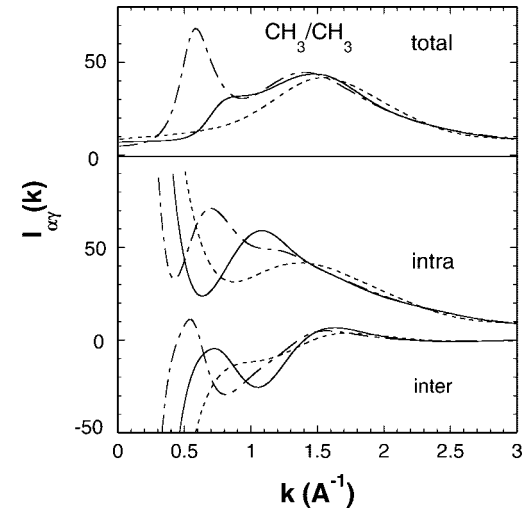

Figure 5. Upper panel shows the partial contributions to the scattering intensity $I_{\alpha\gamma}(k)$ (see eq 12) from CH_3 sites on the side chains calculated as a function of wave vector. In the lower panel the partial scattering is decomposed further into intramolecular and intermolecular contributions. iPP (dashed curves), P1B (solid curves), and P1H (short/long dashed curves).

the pendant group size increases from PE to P1H. Likewise, the CH/CH peak moved with the same trend (0.99, 0.77, and 0.59 Å^{-1}) in proceeding from iPP to P1H. This suggests that the main chains are being forced farther apart as the substituent groups become progressively larger. This is confirmed in the lower part of Figure 4 where the intermolecular radial distribution function $g_{CHCH}(r)$ is plotted. It can be seen that the intermolecular correlation function between backbone sites shifts to larger values of r as the pendant group increased in size. Thus, it appears that the prepeak arises primarily from the chain backbone scattering and shifts to progressively lower wave vectors as the average chain separation increases due to screening effects of the side chains.

Why does peak splitting, rather than a gradual shift of the main peak to lower wave vectors, occur for the vinyl polymers with larger side groups? To address this question, we plotted the scattering contribution due to pairs of CH_3 groups in Figure 5. The upper panel of this figure shows the methyl site scattering of the polymer liquids iPP, P1B, and P1H. It can be seen that, like the total scattering (Figure 2), the methyl contribution itself

displays a splitting in the peak in P1B and P1H but not in iPP. The scattering from pairs of CH_3 moieties is further decomposed into intramolecular ($f_\alpha f_\gamma \hat{\Omega}_{\alpha\gamma}/\rho_\alpha$) and intermolecular ($f_\alpha f_\gamma \hat{H}_{\alpha\gamma}/\rho_\alpha$) contributions in the lower panel of Figure 5. As expected, we observed that the intramolecular scattering between methyl groups shifted to lower wave vectors as the pendant group increased in size resulting from the methyl groups on the same chain being farther apart. On the other hand, the intermolecular contribution to the methyl scattering exhibits increasing structure with the size of the vinyl group. The first intermolecular peak shifts to lower wave vector like the intramolecular peak; however, the second peak stays roughly in the same position at $k \sim 1.6$ Å^{-1}. This increase in intermolecular ordering of the CH_3 groups is confirmed by looking at the intermolecular radial distribution function $g_{\alpha\gamma}(r)$ between methyl groups plotted in the upper portion of Figure 4. As the pendant group becomes larger, we observed a significant increase in the magnitude of the oscillations in the intermolecular radial distribution function reflecting increased intermolecular ordering.

Although we have not shown all the possible partial scattering contributions between the various sites on the polyolefin chains, similar trends were found by studying other pairs of main chain and side chain sites. Thus, it appears that main peak splitting in the X-ray scattering of the vinyl polyolefins arises from an expected shift to lower wave vectors of the main and side chain scattering, coupled with increased intermolecular ordering in the side chains. This effect leads to greater separation in wave vectors between the low angle partial scattering (prepeak), which progressively moves to lower wave vectors, and the second peak of the methyl scattering contribution, which becomes more pronounced and stays roughly in the same position. When the separation in wave vectors from these two scattering sources becomes large enough, the main peak in the total scattering splits into two peaks.

We now present our PRISM predictions for the random copolymers. The statistical mechanics of random copolymers is related to the problem of quenched randomness. An exact treatment would consist of averaging the logarithm of the partition function over all possible sequence distributions that are consistent with a given composition. In previous work, Sung and Yethiraj[37,38] generalized PRISM theory to the case of random copolymers. Because of self-averaging effects in a real random copolymer melt of long chains, these authors pointed out that the random copolymer problem can alternatively be considered an annealed multicomponent chain problem. With standard approximations used in PRISM theory, Sung and Yethiraj found that $\hat{\Omega}_{\alpha\gamma}(k)$ needs to be averaged over all sequence distributions. Using idealized models for the chain architecture, Sung and Yethiraj carried out these calculations for copolymer chains where the intramolecular structure is ideal[37] and also chains where the intramolecular structure is determined self-consistently.[38] For the self-consistent, atomistic model copolymers studied here, averaging $\hat{\Omega}_{\alpha\gamma}(k)$ over all sequence distributions is impractical. Instead, we carry out our PRISM calculations on copolymer chains with a fixed, randomly generated sequence distribution. To assess the sensitivity of the scattering to sequence distribution, we also performed PRISM calculations on copolymer chains with regularly spaced distributions. The sequence distributions and compositions of the three copolymers we studied are summarized in Table 3. We denoted the copolymers of PE and PP as PEP, PE and P1B as PEB, and PE and P1H as PEH.

Since our calculations were carried out self-consistently, we have predictions on the average intramolecular chain dimensions of the melts and copolymers studied here. In particular, we computed the characteristic ratios of the chains defined as $C_n = \langle r^2 \rangle / n\ell^2$, where n is the number of backbone bonds and ℓ is the bond length (1.54 Å). These results are shown in Table 4 for both the random and regular copolymers as a function of composition. Note that the characteristic ratios of the PE and iPP melts ($x = 0$, 1 in Table 4) predicted with PRISM theory are in good agreement with exact MD predictions[2,30] on chains with the same TraPPE force field. It can be seen in Table 4 that the characteristic ratios of corresponding random and regular chains are in close agreement. In the case of the PEP copolymer, C_n varies monotonically with composition between the PE and iPP homopolymers. By contrast, the PEB and PEH copolymers exhibit a minimum characteristic ratio at $x \sim 0.5$.

Table 4. Total Number of Sites/Chain N_T, Number of Backbone Bonds/Chain n, and the Characteristic Ratio C_n Obtained from Self-Consistent PRISM Theory[a]

	PEP random			PEB random			PEH random		
x	N_T	n	C_n	N_T	n	C_n	N_T	n	C_n
0	99	98	8.47 8.36 MD[30]	99	98	8.47	99	98	8.47
0.25	126	111	8.20	100	79	7.21	96	63	7.13
0.50	130	103	7.47	96	63	6.68	112	55	7.08
0.75	132	95	6.89	112	63	7.24	120	47	8.68
1.00	99	65	6.10 5.46 MD[2]	100	49	9.63	96	31	10.03
	PEP regular			PEB regular			PEH regular		
x	N_T	n	C_n	N_T	n	C_n	N_T	n	C_n
0	99	98	8.47	99	98	8.47	99	98	8.47
0.25	99	87	8.16	100	79	7.35	96	63	7.19
0.50	100	79	7.66	96	63	6.44	112	55	6.69
0.75	98	71	6.24	98	55	6.59	120	47	7.33
1.00	99	65	6.10	100	49	9.63	96	31	10.03

[a] The MD values are from refs 30 (PE) and 2 (iPP).

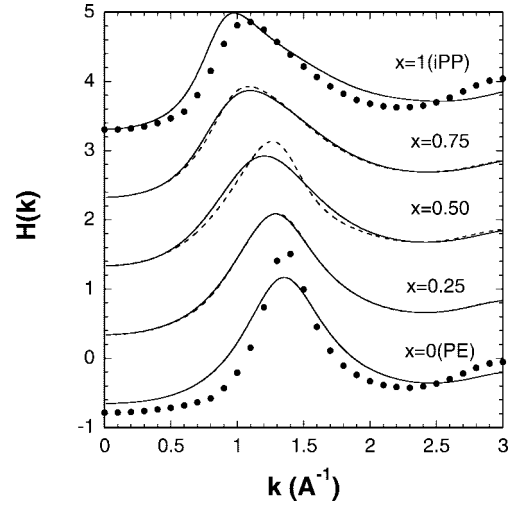

Figure 6. Structure function $H(k)$ (see eq 2) as a function of wave vector k calculated for the PEP random (solid curves) and regular (dashed curves) copolymer at the various compositions indicated. The experimental X-ray scattering results for the pure component PE and iPP melts are denoted by circles. For clarity, the results for each polyolefin are displaced vertically by 1.0.

In Figure 6 we plotted the predicted X-ray scattering for various compositions of the PEP copolymer. Also shown are the corresponding scattering predictions and experimental data for the pure components PE and iPP. It can be seen that the differences between the predicted structure factor of the random (solid curves) and regular (dashed curves) sequences are small in the PEP copolymer. Not surprisingly, the position and breadth of the low angle peak change continuously with composition between PE and iPP. No evidence of a prepeak or peak splitting was found to occur at any composition in PEP.

The corresponding scattering predictions for PEB are plotted in Figure 7. Here we observe that the systems with a random

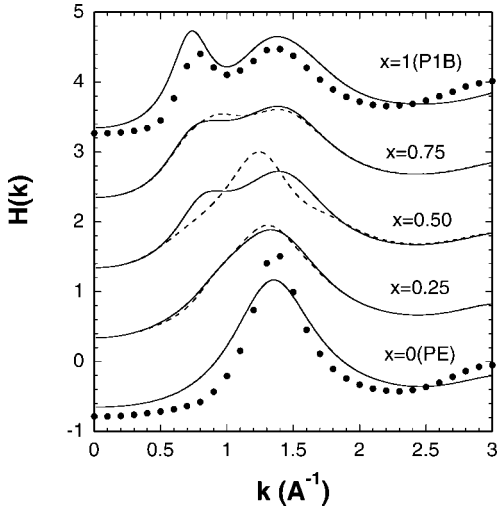

Figure 7. Structure function $H(k)$ (see eq 2) as a function of wave vector k calculated for the PEB random (solid curves) and regular (dashed curves) copolymer at the various compositions indicated. The experimental X-ray scattering results for the pure component PE and P1B melts are denoted by circles. For clarity, the results for each polyolefin are displaced vertically by 1.0.

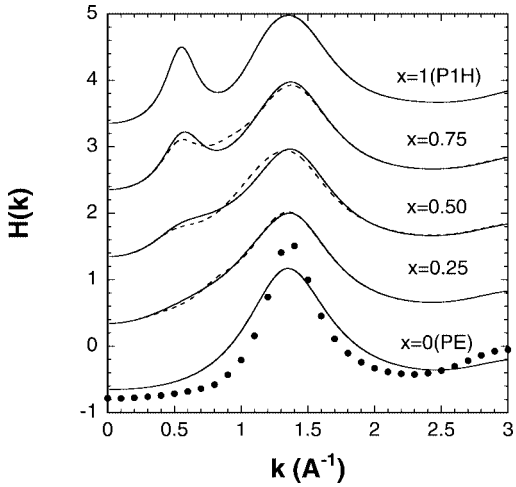

Figure 8. Structure–function $H(k)$ (see eq 2) as a function of wave vector k calculated for the PEH random (solid curves) and regular (dashed curves) copolymer at the various compositions indicated. The experimental X-ray scattering results for the pure component PE melt is denoted by circles. For clarity, the results for each polyolefin are displaced vertically by 1.0.

sequence distribution exhibited peak splitting at $x = 0.50$ and 0.75. By contrast, the regular sequence distribution PEB copolymer appears to have a single broadened peak at $x = 0.50$. Only for this composition was there a significant difference between the random and regular sequences. Examination of the partial contributions from the intramolecular and intermolecular correlation functions does show the initial stages of a prepeak corresponding to greater separation between chain backbones. This smaller contribution, perhaps due to tighter packing arrangements allowed by the regular sequence, results only in a shoulder on the main peak and delays a prepeak until higher copolymer compositions. Finally, in Figure 8 we plotted the equivalent scattering predictions for the random and regular PEH copolymers. In this case PRISM calculations on both the random and regular sequence distribution copolymers predicted that the main angle peak develops a shoulder at $x = 0.50$. At $x = 0.75$ there is a clear peak splitting as in the pure P1H melt.

In summary, our copolymer PRISM calculations predicted scattering curves that gradually change from one pure component to the other. Only in the case of the PEB copolymer at $x = 0.50$ was there any significant sensitivity to the sequence distribution of the repeat units. We are not aware of any wide-angle X-ray scattering measurements on these three copolymer systems at elevated temperatures. It should be pointed out, however, that the PEP copolymer, corresponding to $x = 0.5$ in Figure 6, has been studied through wide-angle X-ray scattering by Londono et al.[1] at room temperature. Consistent with our predictions, no evidence[1] of a prepeak was observed. The experimental results for PEP are not displayed here since the measurements were performed at much lower temperatures, and consequently higher densities, than our calculations. Perhaps future scattering experiments on PEB and PEH will be able to test our predictions regarding the development of a prepeak at intermediate compositions.

Acknowledgment. This work was supported in part by the Division of Materials Sciences, Office of Basic Energy Sciences, U.S. Department of Energy, at the Oak Ridge National Laboratory, managed by UT-Battelle, LLC, for the U.S. Department of Energy under Contract DE-AC05-00OR22725, and at the Sandia National Laboratories, Managed by Lockheed Martin Energy Research Corporation under Contract DE-AC05-840R12400. D.W. also acknowledges Mitsubishi Chemical Corporation for financial support of this work and the NSF (Grant CBET-0731319) during preparation of this manuscript.

References and Notes

(1) Londono, J. D.; Habenschuss, A.; Curro, J. G.; Rajasekaran, J. *J. Polym. Sci., Part B: Polym. Phys.* **1996**, *34*, 3055.
(2) Pütz, M.; Curro, J. G.; Grest, G. S. *J. Chem. Phys.* **2001**, *114*, 2847.
(3) Mitchell, G. R.; Windle, A. H. *Polymer* **1984**, *25*, 906.
(4) Curro, J. G. *Macromolecules* **1994**, *27*, 4665.
(5) Lohse, D. J.; Graessley, W. W. In *Polymer Blends: Formulation and Performance*; Paul, D. R., Bucknall, C. B., Eds.; Wiley: New York, 2000; Vol. *1*, Chapter 8, pp 219−237.
(6) Seki, M.; Nakano, H.; Yamauchi, S.; Suzuki, J.; Matsushita, Y. *Macromolecules* **1999**, *32*, 3227.
(7) Weinmann, P. A.; Jones, T. D.; Hillmyer, M. A.; Bates, F. S.; Londono, J. D.; Melnichenko, Y.; Wignall, G. D.; Almdal, K. *Macromolecules* **1997**, *30*, 3650.
(8) Li, H. Ph.D. Thesis, Colorado School of Mines, **2007**.
(9) Honnell, K. G.; McCoy, J. D.; Curro, J. G.; Schweizer, K. S.; Narten, A.; Habenschuss, A. *J. Chem. Phys.* **1991**, *94*, 4659.
(10) Narten, A.; Habenschuss, A.; Honnell, K. G.; McCoy, J. D.; Curro, J. G.; Schweizer, K. S. *J. Chem. Soc., Faraday Trans.* **1992**, *88*, 1791.
(11) Curro, J. G.; Weinhold, J. D.; Rajasekaran, J. J.; Habenschuss, A.; Londono, J. D.; Honeycutt, J. D. *Macromolecules* **1997**, *30*, 6264.
(12) Kim, M.-H.; Londono, J. D.; Habenschuss, A. *J. Polym. Sci., Part B: Polym. Phys.* **2000**, *38*, 2480.
(13) Cullity, B. D. *Elements of X-ray Diffraction*; Addison-Wesley: Reading, MA, 1956.
(14) Klug, H. P.; Alexander, L. E. *X-ray Diffraction Procedures*, 2nd ed.; Wiley-Interscience: New York, 1974; p 142.
(15) Levy, H. A.; Agron, P. A.; Danford, M. D. *J. Appl. Phys.* **1959**, *30*, 2012.
(16) Narten, A. H.; Levy, H. A. In *Water: A Comprehensive Treatise*; Franks, F., Ed.; Plenum: New York, 1972; Vol. *I*, p 314.
(17) Cromer, D. T.; Mann, J. B. *J. Chem. Phys.* **1967**, *47*, 1893.
(18) Warren, B. E.; Mozzi, R. L. *Acta Crystallogr.* **1966**, *21*, 459.
(19) Narten, A. H. *J. Chem. Phys.* **1979**, *70*, 299.
(20) Curro, J. G.; Schweizer, K. S. *Macromolecules* **1987**, *20*, 1928.
(21) Curro, J. G.; Schweizer, K. S. *J. Chem. Phys.* **1987**, *87*, 1842.
(22) Schweizer, K. S.; Curro, J. G. *Phys. Rev. Lett.* **1987**, *58*, 246.
(23) Chandler, D.; Andersen, H. C. *J. Chem. Phys.* **1972**, *57*, 1930.
(24) Chandler, D. In *Studies in Statistical Mechanics VIII*; Montroll, E. W., Lebowitz, J. L., Eds.; North-Holland: Amsterdam, 1982.
(25) (a) For reviews see: Schweizer, K. S.; Curro, J. G. *Adv. Polym. Sci.* **1994**, *116*, 321. (b) Schweizer, K. S.; Curro, J. G. *Adv. Chem. Phys.*

1997, *98*, 1. (c) Heine, D.; Grest, G. S.; Curro, J. G. *Adv. Polym. Sci.* **2004**, *176*, 211.
(26) Hansen, J. P.; McDonald, I. R. *Theory of Simple Liquids*; Academic Press: London, 1986.
(27) Flory, P. J. *J. Chem. Phys.* **1949**, *17*, 203.
(28) Chandler, D.; Singh, Y.; Richardson, D. M. *J. Chem. Phys.* **1984**, *91*, 1975.
(29) Nichols, A. L.; Chandler, D.; Singh, Y.; Richardson, D. M. *J. Chem. Phys.* **1984**, *81*, 5109.
(30) Heine, D.; Wu, D. T.; Curro, J. G.; Grest, G. S. *J. Chem. Phys.* **2003**, *118*, 914.
(31) Weeks, J. D.; Chandler, D.; Andersen, H. C. *J. Chem. Phys.* **1971**, *54*, 5237.
(32) Martin, M. G.; Siepmann, J. L. *J. Phys. Chem. B* **1998**, *102*, 2569.
(33) Martin, M. G.; Siepmann, J. L. *J. Phys. Chem. B* **1999**, *103*, 4508.
(34) Olabisi, O.; Simha, R. *Macromolecules* **1975**, *8*, 206.
(35) Zoller, P.; Walsh, D. J. *Standard Pressure-Volume-Temperature Data for Polymers*; Technomic Publishing: AG, Basel, 1995.
(36) Elbro, H. S.; Fredenslund, A.; Rasmussen, P. *Ind. Eng. Res.* **1991**, *30*, 2576.
(37) Sung, B. J.; Yethiraj, A. *Macromolecules* **2005**, *38*, 2000.
(38) Sung, B. J.; Yethiraj, A. *J. Chem. Phys.* **2005**, *122*, 234904.

MA702748V